A high-throughput yeast display approach to profile pathogen proteomes for MHC-II binding

Brooke D. Huisman[1,2], Zheng Dai[3,4], David K. Gifford[2,3,4], Michael E. Birnbaum[1,2,5,*]

[1] Koch Institute for Integrative Cancer Research, Cambridge, MA, USA
[2] Department of Biological Engineering, MIT, Cambridge, MA, USA
[3] Computer Science and Artificial Intelligence Laboratory, MIT, Cambridge, MA, USA
[4] Department of Electrical Engineering and Computer Science, MIT, Cambridge, MA, USA
[5] Ragon Institute of MIT, MGH, and Harvard, Cambridge, MA, USA

* Corresponding author: mbirnb@mit.edu

Author contributions

Conception of project: B.D.H. and M.E.B. Conducting experiments: B.D.H. Data analysis: B.D.H. and Z.D. Supervision of work: D.K.G. and M.E.B. Writing manuscript: B.D.H. and M.E.B. Editing manuscript: all authors.

Competing Interest Statement

D.K.G. is a founder of ThinkTx. M.E.B. is an equity holder in 3T Biosciences, and is a co-founder of Viralogic Therapeutics and Abata Therapeutics. The other authors declare no competing interests.

Keywords: yeast surface display, antigen prediction, peptide-MHC

Abstract

T cells play a critical role in the adaptive immune response, recognizing peptide antigens presented on the cell surface by Major Histocompatibility Complex (MHC) proteins. While assessing peptides for MHC binding is an important component of probing these interactions, traditional assays for testing peptides of interest for MHC binding are limited in throughput. Here we present a yeast display-based platform for assessing the binding of tens of thousands of user-defined peptides in a high throughput manner. We apply this approach to assess a tiled library covering the SARS-CoV-2 proteome and four dengue virus serotypes for binding to human class II MHCs, including HLA-DR401, -DR402, and -DR404. This approach identifies binders missed by computational prediction and serves as a framework for diverse objectives, including examining relationships between viral conservation and MHC binding.

Introduction

Major histocompatibility complex (MHC) proteins play a critical role in adaptive immunity by presenting peptide fragments on the surface of cells. Peptide-MHC (pMHC) complexes are then surveilled by T cells via their T cell receptors, enabling immune cells to sense intracellular dysfunction, such as the presence of pathogen-derived peptides. Class I MHCs (MHC-I) present peptides with relatively constrained lengths, typically from 8-11 amino acids, within a closed binding groove to $CD8^+$ cytotoxic T cells. In contrast, class II MHCs (MHC-II) present peptides to $CD4^+$ T cells, and they have an open binding groove, allowing for the display of longer peptides consisting of a 9 amino acid 'core' flanked by a variable number of additional residues on each side.

Generating reliable and rapid data on peptide-MHC binding could be useful for identifying important clinical targets, including for optimized T cell epitopes in vaccine design (Dai et al., 2021; Keskin et al., 2019; Liu et al., 2020, 2021a; Moise et al., 2015; Ott et al., 2017; Patronov and Doytchinova, 2013; Rosati et al., 2021). In fact, therapeutics to generate antigen-specific T cell responses have shown great promise in cancer (Keskin et al., 2019; Ott et al., 2017) and infectious disease (Gambino et al., 2021). Since understanding peptide-MHC binding is critical for identifying and engineering T cell epitopes, there have been sustained efforts to produce high-quality experimental data and predictive algorithms.

Initial experimental methods for determining peptide binding to MHC relied upon the analysis of synthesized candidate peptides via MHC stability or functional assays. While these methods typically produce high-confidence data, they can be difficult to scale beyond a relatively small number of candidate peptides (Altmann and Boyton, 2020; Justesen et al., 2009; Mateus et al., 2020; Sidney et al., 2010; Yin and Stern, 2014). More recently, mass spectrometry-based approaches have been demonstrated for determining the MHC-presented peptide repertoire of cells. These approaches include monoallelic mass spectrometry, which allows for the unambiguous assignment of presented peptides to a given MHC allele. However, mass spectrometry-based approaches are not necessarily quantitative measures of presented peptide affinity or abundance, although there have been advances in quantitation using internal standards (Stopfer et al., 2020, 2021). Additionally, peptides naturally expressed by a cell can potentially crowd out exogenously examined peptides of interest (Abelin et al., 2017, 2019; Parker et al., 2021; Purcell et al., 2019).

A wave of higher throughput approaches have been recently developed for studying peptide-MHC interactions, including yeast display (Jiang and Boder, 2010; Liu et al., 2021b; Rappazzo et al., 2020) and mammalian display-based methods (Obermair et al., 2021). Several of these approaches circumvent the bottlenecks of synthesizing or identifying peptides by utilizing DNA-based inputs and outputs (Jiang and Boder, 2010; Obermair et al., 2021; Rappazzo et al., 2020). These assays rely upon libraries that are often generated via DNA oligonucleotide synthesis, and use peptide stabilization and surface expression (Jiang and Boder, 2010; Liu et al., 2021b; Obermair et al., 2021) or peptide dissociation (Rappazzo et al., 2020) to assess peptide-MHC binding.

In addition to experimental advances, computational approaches for peptide-MHC binding prediction have advanced markedly over the past decade. These developments are due to algorithmic advances (O'Donnell et al., 2020; Racle et al., 2019; Reynisson et al., 2020; Zeng and Gifford, 2019) and the availability of large, high-quality training data (Abelin et al., 2017,

2019; Rappazzo et al., 2020; Reynisson et al., 2020). However, despite the improvements in predicting peptide binding to MHC in a broad sense, the predictive power for individual peptides often remain imperfect relative to experimental measurements (Rappazzo et al., 2020; Zhao and Sher, 2018).

Here we present a yeast display approach to directly assess peptide-MHC binding for large collections of defined peptide antigens, by adapting a previously described MHC-II platform (Rappazzo et al., 2020) to screen whole viral proteomes for MHC-II binding in high-throughput. We utilize this approach to screen the full proteome of SARS-CoV-2, a present, global threat to public health. We additionally apply this approach to screen proteomes from serotypes 1-4 of dengue viruses, in which antibody dependent enhancement results in more severe disease upon second infection with a different serotype of the virus (Guzman et al., 2016), and thus represents a potential important application area for T cell-directed therapeutics.

Results

Generation of yeast display libraries for profiling the SARS-CoV-2 proteome

Previous studies have reported the use of yeast-displayed MHC-II for characterizing peptide-MHC and pMHC-TCR interactions (Birnbaum et al., 2014, 2017; Rappazzo et al., 2020). We adapted MHC-II yeast display constructs (Rappazzo et al., 2020) to generate a defined library of peptides that cover the SARS-CoV-2 proteome to assess them for MHC binding. To compare SARS-CoV-2 with a related coronavirus, we also included peptides from the spike and nucleocapsid proteins from SARS-CoV.

Each protein was windowed into peptides of 15 amino acids in length, with a step size of 1 **(Figure 1a)**, and each peptide was encoded in DNA and cloned in a pooled format into yeast vectors containing MHC-II proteins. The generated library was linked to three MHC-II alleles: HLA-DR401 (HLA-DRA1*01:01, HLA-DRB1*04:01), HLA-DR402 (HLA-DRA1*01:01, HLA-DRB1*04:02), and HLA-DR404 (HLA-DRA1*01:01, HLA-DRB1*04:04). Yeast were formatted as previously described (Rappazzo et al., 2020), where a flexible linker connecting the peptide and MHC contains a 3C protease site and a Myc epitope tag, which can be used for selections **(Figure 1a)**. The final library contained 11,040 unique peptides, with 99% of the designed peptides present in each cloned yeast library, as assessed by next-generation sequencing.

Strategies for selecting defined libraries

To enrich for peptide binders, iterative selections were performed as previously described (Rappazzo et al., 2020) (**Figure 1a**): the library is first incubated with competitor peptide and 3C protease, which cleaves the covalent linkage between peptide and MHC, followed by the addition of HLA-DM at lower pH. These conditions allow for the encoded peptide to be displaced from the peptide-binding groove. The Myc epitope tag is proximal to the peptide, which can be identified via incubation with an anti-epitope tag antibody followed by enrichment via magnetic bead selection if the yeast-expressed peptide remains bound to the MHC after the peptide exchange reaction.

Three rounds of selection were iteratively performed. Representative enrichment of yeast expressing Myc-tagged peptides can be seen in **Figure 1c** ("undoped library"), for the library displayed by HLA-DR401. Here the pre-selection Myc-positive population starts at 29.3%

126 and quickly converges, with 65.0% positive in the pre-selection Round 2 population and 74.1%
127 in the pre-selection Round 3 population.
128 Given the rapid convergence of the library, we performed a second set of selections in
129 which we doped the defined library into a randomized, null library to enable a greater degree of
130 enrichment as compared to non-binding peptides. The null library was generated by fully
131 randomizing ten amino acids in the peptide region of the peptide-MHC-II construct while fixing
132 three amino acids to encode stop codons. This library provides a baseline population of yeast
133 which should not express pMHC, and therefore not enrich in our selections. We doped our
134 defined peptide library into a 500-fold excess of null library, such that each peptide member
135 was represented at approximately the same frequency (**Figure 1b**). The null library provides
136 baseline competition, which true binders must enrich beyond, and increases the stringency of
137 the enrichment task.
138 We performed four rounds of selection on the doped library. Because of the excess of
139 null yeast, the initial pre-selection stain is low (1.6%) compared to the initial undoped library
140 (**Figure 1c**). This staining enriched over the first three rounds of selection, reflective of the
141 stringency of the task and clarity of enrichment. This is in contrast to the initial undoped library,
142 which began with a much higher pre-selection stain, with a lower fold-change in staining over
143 rounds of selection. The low frequency of each member in the starting doped library, however,
144 increases the likelihood of stochastic dropout for any given member.
145
146 *Analysis of selection data*
147 After selections, peptide identities were determined through deep sequencing of
148 enriched yeast populations, providing us with a dataset comprised of positive enrichment over
149 four rounds of selection from the doped library and both positive and negative enrichment for
150 three rounds of selection from the undoped library (**Supplemental Data**). **Supplemental Figure**
151 **1** shows the correlation between defined library members on HLA-DR401. As expected, the
152 unselected library correlated poorly with post-selection rounds. Consistent with the observed
153 staining (**Figure 1c**), the doped library essentially converged after Round 3, making it likely that
154 changes between Rounds 3 and 4 were due to stochastic variation rather than improved
155 binding. Similarly, the undoped library appears converged following Round 2.
156 Next, we established metrics for enrichment for each mode of selection. Given the high
157 starting frequency of members in the undoped library, we classify enrichment based on fold
158 change between Round 1 and Round 2, and we define criteria for enriched yeast in the
159 undoped library as making up a higher fraction of reads following Round 2 compared to Round
160 1. In contrast, in the doped library, members start at low frequencies, and we define
161 enrichment based on presence above a threshold in Round 3 of selection, specifically as having
162 greater than or equal to 10 reads following Round 3. **Figure 2b** illustrates the correspondence
163 between enrichment metrics in the doped and undoped library for the library on HLA-DR401.
164 Of the 11,040 peptides in the library, 2,467 enriched in both the doped and undoped libraries
165 displayed by HLA-DR401 (**Figure 2a**). An additional 1,252 enriched in the doped library only and
166 797 enriched in the undoped library only.
167 In further data analysis, we identified a potentially confounding factor caused by the
168 construct design itself: the N-terminus of the peptide includes an extra alanine to ensure
169 consistent cleavage between the construct and its signal peptide, while the C-terminus of the

170 peptide is connected to the MHC construct via a Gly-Ser linker (**Figure 1a**). Since each 15mer
171 peptide is flanked by invariant sequences that are not present in the native sequences, it is
172 possible that individual peptide-construct fusions may produce high-affinity peptide binding
173 registers that do not occur natively. The small residues comprising the Gly-Ser linker are
174 favorable anchor residues at position 9 for each MHC allele in our study (Abelin et al., 2019;
175 Rappazzo et al., 2020; Reynisson et al., 2020). As a result, there are three non-native registers in
176 which a peptide could utilize a linker residue as a position 9 anchor without using a linker
177 residue at the position 6 anchor, which does not favor Gly or Ser (Abelin et al., 2019; Rappazzo
178 et al., 2020; Reynisson et al., 2020). In setting a threshold for high confidence enrichment, we
179 therefore sought to exclude peptides which rely on non-native linker residues in the groove for
180 enrichment.
181 Because the library is designed with a step size of one, we utilized redundancy between
182 adjacent peptides to determine high-confidence binders, including adjusting for peptides which
183 enrich with linker residues in the groove. To do this, we implement a smoothing method,
184 examining overlapping peptides for shared enrichment behavior. Classically, the strongest
185 determinant of peptide affinity for an MHC is the nine amino acid stretch sitting within the
186 peptide-binding groove (Jones et al., 2006; Stern, 1994), although proximal peptide flanking
187 residues can also affect binding (Lovitch et al., 2006; O'Brien et al., 2008; Zavala-Ruiz et al.,
188 2004). In our libraries, a given 9mer is present in seven overlapping 15mer peptides, and we
189 calculate how many of these seven 15mers have enriched. This calculation is shown
190 schematically in **Supplemental Figure 2a** with toy sequences and applied to enrichment data
191 for SARS-CoV-2 nucleocapsid on HLA-DR401 in **Supplemental Figure 2b**. Sequences with good
192 9mer cores should enrich along with neighboring sequences with the same 9mer sequence. In
193 contrast, sequences which enrich spuriously or due to linker sequence in the peptide groove or
194 other stochastic factors should have few neighbor sequences also enriching. Thus, we define a
195 cutoff for high confidence 9mer enrichment of five out of seven 9mer-containing sequences
196 enriching. This cutoff tolerates some stochastic dropout, while being above the probable sets of
197 three peptides that could enrich only with the Gly-Ser in the Position 9 pocket. Of the 2,467
198 peptides which enriched in both the doped and undoped libraries for HLA-DR401, 1,791 also
199 contain a 9mer sequence which enriched in five or more peptides of the seven neighboring
200 sequences containing it (**Figure 2a**), with 676 peptides enriching in both doped and undoped
201 libraries but not containing a 9mer core enriched in five or more peptides, and 788 15mers
202 containing a 9mer which enriched in five or more peptides but enriched in zero or one of the
203 doped and undoped libraries. These full relationships are captured in Venn diagrams in
204 **Supplemental Figure 3** for all three MHC alleles studied here.
205
206 *Sequence motifs of enriched peptides are consistent with known binders*
207 To examine the 9mer core motifs of enriched peptides, we utilized a position weight
208 matrix method to infer the peptide register and generated visualizations of the 9mer cores
209 using Seq2Logo (Thomsen and Nielsen, 2012). **Figure 2c** shows a sequence logo of the aligned
210 9mer cores from the 2,467 15mer peptides which enriched on HLA-DR401 in both doped and
211 undoped libraries. The peptide motif is consistent with previously reported motifs for HLA-
212 DR401 (Abelin et al., 2019; Rappazzo et al., 2020): hydrophobic amino acids are preferred at P1,
213 acidic residues at P4, polar residues at P6, and small residues at P9. We also observe some

214 preference for glycine at P8 in the sequence logo, which is potentially an artifact of non-native
215 registers with linker at P8 and P9.
216 The other alleles used in the study, HLA-DR402 and HLA-DR404, have polymorphisms in
217 their peptide binding groove sequences as compared to HLA-DR401, which affect binding
218 preferences. HLA-DR401 differs from HLA-DR402 at four amino acids and from HLA-DR404 at
219 two amino acids, with all polymorphisms located in the beta chain. HLA-DR402 and HLA-DR404
220 share an amino acid distinct from HLA-DR401 affecting the P1 pocket (Gly86Val), resulting in a
221 preference for smaller hydrophobic residues (**Figure 3a**). Three polymorphisms in HLA-DR402
222 affect P4, P5, and P7 compared to HLA-DR401 (Leu67Ile, Gln70Asp, and Lys71Glu), while HLA-
223 DR404 has only one (Lys71Arg). Sequence logos for HLA-DR402 and HLA-DR404 are consistent
224 with previously reported motifs and MHC polymorphisms (**Supplemental Figure 4**). We observe
225 less P4 preference compared to the motif of HLA-DR402 binders enriched from a randomized
226 yeast display peptide library (Rappazzo et al., 2020), albeit consistent with mass spectrometry-
227 generated motifs which also showed minimal P4 preference for HLA-DR402 (Abelin et al.,
228 2019).
229 To probe the diminished P4 peptide preference observed for HLA-DR402 and HLA-
230 DR404, we examined differences between the compositions of randomized and defined
231 libraries. We hypothesized that skewed amino acid abundances in nature, which are reflected
232 in the defined library, could result in an apparent diminished amino acid preference. Indeed,
233 three of the most preferred P4 residues for binding HLA-DR402, Trp, His, and Met (Rappazzo et
234 al., 2020), are all low abundance in the SARS-CoV-2 proteome (Trp 1.1%, His 1.9%, Met 2.2%). In
235 comparison, a randomized peptide library for HLA-DR402 (Rappazzo et al., 2020) had a higher
236 representation of these amino acids (Trp 3.8%, His 2.9%, Met 3.8%). Additionally, the
237 randomized library had approximately nine thousand-fold more members than the defined
238 library, providing more instances of all amino acids. The low abundance and
239 underrepresentation of these amino acids likely underlies the apparent lack of amino acid
240 consensus at P4 in enriched peptides. Interestingly, Arg and Lys, which have also been reported
241 as preferred HLA-DR402 P4 residues, are more abundant than Trp, His, and Met in the SARS-
242 CoV-2 proteome (Arg 3.4% and Lys 5.9%; compare to Arg 9.7%, Lys 4.0% in the random library),
243 but still show less representation at P4 in the defined library enriched peptides compared to
244 the random library-enriched peptides. These differences in motifs between randomized and
245 defined libraries highlight the utility of randomized libraries for downstream applications such
246 as training prediction algorithms. Approaches influenced by amino acid abundance in nature,
247 such as defined libraries and mass spectrometry approaches, could inadvertently bias against
248 possible binders because of absence of amino acids in their null distribution, rather than true
249 binding preference.
250 Next, we wanted to examine the distribution of peptides among the possible 9mer
251 registers along each 15 amino acid sequence. Based on our register inference, of the 2,467
252 enriched peptides from the HLA-DR401 library, 1,610 peptides bound native 9mer cores
253 without using any linker sequence residues in the 9mer core, which is consistent with
254 theoretical ratios of possible native and non-native cores for a given 9mer (**Supplemental**
255 **Data**). The peptides with predicted native 9mer cores were approximately equally distributed
256 between possible registers, with the exception of the N-terminal register, which had one-third
257 fewer peptides. This register had only a single N-terminal flanking residue (the fixed Ala), which

258 is likely disfavored. We also identified a register with the linker filling positions 6 through 9 in
259 the groove, though this is the least frequent register, with 118 peptides.
260 Because the library was designed with step size of one, many of the 9mer cores will be
261 repeated among neighboring peptides. Of the 1,610 HLA-DR401 peptides which enriched using
262 a native 9mer core, there are 563 unique 9mer cores identified through register-inference.
263 **Table 1** summarizes enrichment for each protein included in the library, highlighting the
264 number of 15mers which enriched in both the doped and undoped libraries, the number of
265 unique native 9mer cores, and the number of 15mers containing a 9mer enriched in at least
266 five of seven overlapping peptides.
267
268 *MHC-specific relationships can be observed in binding to library peptides: MHC binding to SARS-*
269 *CoV and SARS-CoV-2 spike proteins*
270 To further explore relationships between the MHCs studied here and their virally-
271 derived peptide repertoires, we compared the binding of SARS-CoV-2 and SARS-CoV spike
272 proteins to all three MHC alleles. Sequence alignment of these three MHC alleles is shown in
273 **Figure 3a**, with polymorphic regions highlighted on an HLA-DR401 structure (adapted from PDB
274 1J8H). Interplay between viral conservation and binding are illustrated in **Figure 3b**, highlighting
275 conserved regions of the proteome in black and binders to each allele in grey, red, and blue.
276 Regions are highlighted where sequences enrich in overlapping peptides; that is, for each 9
277 amino acid stretch along the proteome, we calculated how many of the seven 15mer peptides
278 enrich in the yeast display assay, and if a 9mer enriched five or more times, it is marked as a hit.
279 Specific examples of these relationships are probed in **Figure 3c, d, and e**, where individually
280 enriched 15mer sequences are represented as horizontal lines above 15mer stretches in the
281 proteome. Bolded 9mers are identified through register inference as consensus binding cores
282 for these peptides. Only 15mers which contain the bolded 9mer are included in this
283 representation. Non-conserved amino acids within this 9mer are highlighted in yellow.
284 **Figure 3c** illustrates a region that is not conserved between SARS-CoV-2 and SARS-CoV,
285 where the SARS-CoV-2 peptides containing the core IYQAGSTPC are enriched for binding to all
286 three MHCs, but mutations, including at both P1 and P4 to Proline, discourage binding of the
287 aligned SARS-CoV peptide. **Figure 3e** illustrates a core that is conserved between SARS-CoV and
288 SARS-CoV-2, which can bind only to HLA-DR401, but not to HLA-DR402 or HLA-DR404, likely due
289 to the size of the P1 hydrophobic residue and, for HLA-DR402, the acidic P4 residue. **Figure 3d**
290 illustrates relationships between both viral conservation and MHC preference. In **Figure 3d**, the
291 SARS-CoV peptides containing the core IKNQCVNFN can bind to all three alleles. However, the
292 aligned SARS-CoV-2 peptides containing the core VKNKCVNFN do not bind to HLA-DR401, likely
293 because of the less preferable P1 Valine and basic P4 Lysine, but can bind to HLA-DR402, which
294 prefers these residues. These peptides can bind to HLA-DR404, although only four of the
295 adjacent peptides containing this core enrich, which is below the cutoff of five or more, and
296 since no other adjacent peptides enriched, this would not have been classified as a binder
297 (reflected in **Figure 3b**). This marginal, but below-threshold binding is logical, given that the P4
298 pocket for HLA-DR404 is similar to HLA-DR401, which does not prefer P4 Lysine, but HLA-DR404
299 has the same P1 binding pocket as HLA-DR402, which both prefer the P1 Valine in the SARS-
300 CoV-2 peptide.
301

302 *Comparing enriched sequences and algorithm predictions*
303 Next, we compared our direct experimental assessments with results from
304 computational MHC binding predictions. Prediction algorithms allow for rapid computational
305 screening of potential peptide binders (Abelin et al., 2019; Reynisson et al., 2020), although
306 they can contain systemic biases (Rappazzo et al., 2020). To test the outputs of our direct
307 assessment approach and computational prediction algorithms, we assessed binding of several
308 peptides using a fluorescence polarization competition assay to determine IC_{50} values, as
309 described previously (Rappazzo et al., 2020; Yin and Stern, 2014). Yeast-formatted peptides
310 (Ala+15mer+Gly+Gly+Ser) from SARS-CoV-2 spike protein were run through NetMHCIIpan4.0
311 for binding to HLA-DR401, with binders defined as having $\leq$ 10% Rank (Eluted Ligand mode).
312 Yeast display binders to HLA-DR401 were defined via the stringent criteria of 1) enriching in
313 both in doped and undoped selections, and 2) containing a 9mer that enriched in five or more
314 of the overlapping seven 15mers. 15mers were selected such that they could contain a
315 maximum overlap of 8 amino acids with other selected peptides, to avoid selecting peptides
316 with redundant 9mer cores. An length-matched version of the commonly studied Influenza A
317 $HA_{306-318}$ peptide (APKYVKQNTLKLATG) known to bind HLA-DR401 (Hennecke and Wiley, 2002;
318 Rappazzo et al., 2020) was included as a positive control, along with sequences that yeast
319 display and NetMHCIIpan4.0 both classified as either binders or non-binders. **Supplemental**
320 **Figure 5** shows a comparison of yeast-enriched and NetMHCpan4.0 predicted binders, with
321 boxed sequences selected for testing by fluorescence polarization.
322 The resulting fluorescence polarization IC_{50} data from the native 15mer peptides are
323 shown in **Table 2** and **Supplemental Figure 6**. Peptides which both enriched in yeast display and
324 were predicted by NetMHCIIpan4.0 to bind ('Agreed Binders') all showed IC_{50} values consistent
325 with binding, each with $IC_{50} < 2.2$ µM. Similarly, peptides which were agreed non-binders
326 showed no affinity for HLA-DR401, with $IC_{50} > 50$ µM.
327 All 8 'Yeast-Enriched Binders', which enriched in the yeast display assay but were not
328 predicted to bind via NetMHCIIpan4.0, showed some degree of binding, with IC_{50} values
329 distributed from 14 nM (higher affinity than the HA control peptide) to 18 µM (weak, but
330 measurable, binding). Retrospectively, the weakest two binders appear to be enriching in the
331 yeast assay using the peptide linker or have a binding core offset from center. Interestingly,
332 NetMHCIIpan4.0 predictions on the peptides identified via yeast display proved highly sensitive
333 to the length or content of the flanking sequences: if we repeat predictions on only the antigen-
334 derived 15mer sequences without the flanking sequences, NetMHCIIpan4.0 recovers four of its
335 former false negative peptides (**Table 3**; peptides listed at the top in each section of the table).
336 We will refer to these four peptides as 'flank-sensitive centered peptides', as they each have
337 the consensus 9mer core centered in the peptide.
338 To further investigate the relationship with flanking residues, we selected five additional
339 peptides ('offset peptides') matching three criteria; these offset peptides were 1) enriched in
340 the yeast display assay, 2) share an overlapping core with the four flank-sensitive centered
341 peptides, but are 3) not predicted by NetMHCIIpan4.0 to be binders (either with or without
342 invariant flanking sequence added). All five offset peptides have their predicted cores offset by
343 1-2 amino acids from center, leaving at minimum 1 amino acid on both ends of the 9mer core
344 for each peptide. All five offset peptides exhibit some binding, with IC_{50} values below 13 µM,
345 although each peptide is lower affinity than its overlapping centered counterpart, illustrating

346 effects of flanking residues on peptide binding, although some over-estimation of these effects
347 in NetMHCIIpan4.0 predictions are present.
348 We tested three 'NetMHC-Predicted Binders', which were predicted to bind by
349 NetMHCIIpan4.0, but were not enriched (nor did any neighboring sequences within an offset of
350 4 amino acids) in the yeast display assay (**Table 2**). Of these, one bound to HLA-DR401 (IC_{50} 475
351 nM), while two showed minimal binding with IC50 > 35 µM, which is above the maximum 20
352 µM concentration tested. All three were predicted by NetMHCIIpan4.0 to bind with or without
353 the invariant flanking sequences (Eluted ligand mode % Rank: 5.7, 4.1, 8.7 (with flanking
354 residues) and 2.3, 0.6, 7.0 (without flanking residues), for ELDKYFKNHTSPDVD,
355 LQSYGFQPTNGVGYQ, and KTQSLLIVNNATNVV, respectively).
356 Of the eight 'Yeast-Enriched Binders' in **Table 2**, six contain cysteine residues, which
357 have been shown to be systematically absent from other datasets, including those from mono-
358 allelic mass spectrometry (Abelin et al., 2019; Barra et al., 2018), yet present in yeast display-
359 derived datasets (Rappazzo et al., 2020). To test for non-specific binding due to cysteine, two
360 cysteine-containing 'Agreed Non-Binders' were also tested and showed no affinity for HLA-
361 DR401, suggesting that cysteine itself is not causing non-specific binding. In the fluorescence
362 polarization dataset, the highest affinity binder (14 nM) contained cysteine and was missed by
363 NetMHCIIpan4.0 predictions (Eluted ligand mode % Rank: 71 (with flanking residues) and 28
364 (without flanking residues)).
365 The relationship between measured IC_{50} values and NetMHCIIpan4.0 predicted values
366 for all 15mer SARS-CoV-2 spike peptides tested is shown in **Figure 4** and **Supplemental Figure 7**.
367
368 *Yeast display approach can be used to compare dengue serotypes for MHC binding*
369 Defined yeast display libraries can generate data for diverse objectives. Dengue viruses
370 typically cause most severe disease after a second infection with a serotype different from the
371 first infection, due to antibody dependent enhancement (Guzman et al., 2016), which makes T
372 cell-directed therapeutics a potentially attractive means of combatting disease. To profile and
373 compare MHC binding across serotypes, we generated libraries containing 12,672 dengue-
374 derived peptides, covering the entire proteomes of dengue serotypes 1-4. These libraries were
375 on HLA-DR401 and HLA-DR402 and had coverage of 98% and 96% of the dengue library
376 members after construction, respectively.
377 Peptides from homologous regions of the four dengue serotypes have different MHC
378 binding ability, as illustrated in **Figure 5a** for binding to HLA-DR401. The proteins encoded in the
379 dengue genome are indicated along the horizontal axis (C: capsid; M: membrane; E: envelope;
380 NS: nonstructural proteins). Peptides that enriched in the yeast display assay are marked by a
381 line (serotype 1 in blue, serotype 2 in purple, serotype 3 in red, and serotype 4 in grey). The
382 proteome is smoothed to 9 amino acid stretches (as in **Figure 3b**), with a given 9 amino acid
383 region marked as a hit if five or more of the seven adjacent peptides enrich. For each 9mer, the
384 maximum number of serotypes with a conserved identical 9mer at that position is indicated at
385 the top in black.
386 These data can reveal relationships between conservation and binding ability. **Figure 5b-**
387 **d** shows enrichment data for individual 15mer peptides, with consensus inferred 9mer cores in
388 bold and non-conserved amino acids in these cores highlighted in yellow, as in **Figure 3c-e**.
389 Conserved cores which show binding ability (**Figure 5c**) may be ideal T cell targets. However,

390 the permissiveness of the binding groove allows for peptides to bind that have mutations at the
391 anchors, such as in NS5 (**Figure 5d**), where P4 Asn and P4 Met both allow binding. Interestingly,
392 the serotype 3 core (LASNAICSA) only enriched in four peptides, which is below our described
393 cutoff for high-confidence peptide cores. However, three adjacent peptides enriched and
394 register-inference for these peptides identifies the non-native, linker-containing version of the
395 LASNAICSA core as binding in the MHC-binding groove. This results in an adjacent 9mer being
396 highlighted as a binder in this region (**Figure 5a**) because overlapping 15mers enrich in five or
397 more of the seven adjacent peptides. With this in mind, care must be taken for core
398 identification in enriched regions and can be aided by coupling enrichment with register-
399 inference of enriched peptides. Further, we can also see relationships between conservation
400 and binding in non-conserved regions, such as in the envelope protein (**Figure 5b**) with the
401 mutations in serotype 3 enabling binding.
402
403 **Discussion**
404 $CD4^+$ T cells responses play important roles in infection, autoimmunity, and cancer. By
405 extension, understanding peptide-MHC binding is critical for identifying and engineering T cell
406 epitopes. Here we present an approach to directly assess defined libraries of peptides covering
407 whole pathogen proteomes for binding to MHC-II proteins. We examine alternative modes of
408 selection and utilize overlapping peptides to determine high-confidence binders. We
409 demonstrate the utility of this approach by identifying binders that are missed by prediction
410 algorithms, highlighting a prediction algorithm bias against cysteine-containing peptides and
411 sensitivity to peptide flanking residues (**Table 2** and **Table 3**). Finally, this approach can be
412 utilized for different objectives, including comparing binding to multiple MHC alleles (**Figure 3**)
413 or comparing peptides from related pathogen sequences for MHC-II binding (**Figure 5**).
414 This approach for direct assessment shows benefit compared to prediction algorithms
415 for identifying binders, particularly for finding weak peptide binders. The overlapping peptides
416 in our library were useful for identifying enriched cores, especially when combined with register
417 inference to identify consensus cores shared between these overlapping peptides.
418 NetMHCIIpan4.0 exhibits a sensitivity to length and register, which may cause users to miss
419 binders, albeit potentially of lower affinity. Of the overlapping peptides we tested to study this
420 phenomenon, NetMHCIIpan4.0 correctly ranked the affinities of the overlapping peptides
421 (**Table 3**), but missed binders. **Supplemental Figure 5** also highlights the sensitivity of
422 NetMHCIIpan4.0 to flanking sequences, where neighboring peptides with shared cores often
423 are not predicted to bind, resulting in fewer clusters of peptides in **Supplemental Figure 5**.
424 Design of defined libraries with sources of redundancy, such as overlapping peptides,
425 was critical for determining binders with higher degrees of confidence and allowed us to apply
426 stringent cutoffs for individual peptides. Overlapping peptides allowed us to account for
427 construct-specific confounding effects, such as the peptides binding using non-native residues
428 in the linker. Future iterations can change the sequence of the linker, such as defining favorable
429 P-1 and P10 anchors to fix the register (Rappazzo et al., 2020), although these adaptations
430 would likely require MHC-specific knowledge in advance and may need to be altered for
431 different MHCs. Additionally, the engineered redundancy and multiple modes of selection
432 result in hyperparameters that can be tuned to meet users' stringency requirements, such as

433 defining different thresholds for calling individual 15mer binders or alternative integration of
434 overlapping binders.
435 Further, this approach can be used to study MHC binding between similar viruses, as
436 done with the dengue proteomes and the spike proteins from SARS-CoV-2 and SARS-CoV,
437 highlighting regions where mutations disrupt binding as well as regions where binding is
438 unperturbed. This method can also be rapidly adapted to study future sequences if pathogens
439 evolve over time.
440 As experimental approaches and computational approaches continue to co-develop,
441 they present complementary benefits. Though this platform allows for rapid assessment of
442 peptide-MHC binding, the speed of computational prediction surpasses experimental
443 approaches. NetMHCIIpan4.0 prediction and yeast display selections identified sets of non-
444 overlapping misses, highlighting a utility for both. Additionally, all agreed binders and non-
445 binders matched fluorescence polarization results, suggesting a consensus of yeast display
446 enrichment and algorithmic prediction provide high-confidence results. Approaches such as
447 yeast display assessment can be used to complement computational approaches, such as for
448 identifying cysteine-containing peptides which are still under-predicted by algorithms. Similarly,
449 prediction algorithms can be trained using large, quality datasets to account for biases. In
450 another application, our platform to assess peptide-MHC binding can be used to design high-
451 throughput assays to test peptide immunogenicity in clinical samples (Klinger et al., 2015;
452 Snyder et al., 2020).
453 Defined yeast display peptide libraries can also be readily applied to identification of T
454 cell ligands and present an opportunity for identifying unknown ligands from orphan TCRs
455 known to respond to a proteome of interest (Birnbaum et al., 2014; Gee et al., 2018). Indeed, as
456 DNA synthesis and sequencing continue to advance, defined peptide libraries expanding
457 beyond viral proteomes to covering whole bacterial or human proteomes will be possible, and
458 could present opportunities for investigating autoimmune diseases, which frequently have
459 strong MHC-II associations (Karnes et al., 2017). Such tools would be rich resources for
460 identifying both peptide-MHC binders and TCR ligands.

Methods

Library design and creation

Yeast display libraries were designed to cover all 15mer sequences within a given proteome, with step size one. Reference proteomes used in creating defined libraries were accessed from Uniprot, with the following Proteome IDs. SARS-CoV-2: UP000464024, SARS-CoV: UP000000354, dengue serotype 1: UP000002500, dengue serotype 2: UP000180751, dengue serotype 3: UP000007200, dengue serotype 4: UP000000275. The dengue proteome is expressed as a single polypeptide, and peptides were generated from that contiguous stretch.

Each library peptide is encoded in DNA space, with specific codons selected randomly from possible codons, with probabilities matching yeast codon usage (GenScript Codon Usage Frequency Table). The DNA-encoded peptide sequences were flanked by invariant sequences from the yeast construct for handles in amplification and cloning, and the DNA oligonucleotide sequences were ordered from Twist Bioscience (South San Francisco, CA), with maximum length of 120 nucleotides. The DNA oligo pool was amplified in low cycle PCR, followed by amplification with construct DNA using overlap extension PCR. This extended product was assembled in yeast with linearized pYal vector at a 5:1 insert:vector via electroporation with electrocompetent RJY100 yeast.

HLA-DR401 and HLA-DR402 libraries were generated using previously described vectors (Rappazzo et al., 2020) which contain mutations from wild type Metα36Leu, Valα132Met, Hisβ33Asn, and Aspβ43Glu to enable proper folding without disrupting TCR or peptide contact residues (Birnbaum et al., 2017). HLA-DR404 was generated using the same stabilizing mutations.

The previously described null library (Dai et al., 2021) was generated with a peptide encoded as “NNNTAANNNNNNNNNTAGNNNNNNNNNNNNTGANNNNNN”, where “N” indicates any nucleotide and encodes ten random amino acids and three stop codons. This library was similarly generated in yeast using electrocompetent RJY100 yeast.

Peptide visualizations and predictions

Data visualizations of viral conservation and enrichment were generated using custom scripts. For each 9mer stretch in a protein of interest, there are seven 15mer sequences that overlap and contain that 9mer. We calculate how many of these seven 15mers enriched in both the doped and undoped libraries. If five or more of the seven 15mers enriched, that stretch is marked as a ‘hit’. To examine conservation between viruses, viral proteins are aligned using ClustalOmega (Madeira et al., 2019). Aligned 9mer stretches are compared between viruses and identical stretches are considered conserved. Hits are determined individually for each virus before merging, such that gaps in sequence alignments do not affect calculations of enrichment for a given virus.

Representations of 15mer hits (as in **Figure 3**, **Figure 5** and **Supplemental Figure 5**) were generated using in-house scripts, such that a 15mer that enriched in both the doped and undoped library was marked as a horizontal line above the relevant 15mer sequence. Only 15mers containing the bolded 9mer in **Figure 3** and **Figure 5** were included.

NetMHCIIpan4.0 webserver was used for computational predictions (Reynisson et al., 2020), where a binder is defined as having a predicted percent rank ≤ 10%, as defined in the webserver instructions.

505
506 *Yeast library selections*
507 Library selections were consistent with previous peptide-MHC-II yeast display
508 dissociation studies (Dai et al., 2021; Rappazzo et al., 2020). Yeast were washed into pH 7.2 PBS
509 to a concentration with 1 µM 3C protease and incubated at room temperature for 45 minutes.
510 Yeast were then washed into 4 °C acid saline (150mM NaCl, 20mM citric acid, pH5) with 1 µM
511 HLA-DM and incubated at 4 °C overnight. Each step takes place in the presence of competitor
512 peptide (HLA-DR401: $HA_{306-318}$ PKYVKQNTLKLAT, 1 µM; HLA-DR402: $CD48_{36-51}$
513 FDQKIVEWDSRKSKYF, 5 µM; HLA-DR404: NKVKSLRILNTRRKL, 5 µM (Vita et al., 2019)). Non-
514 specific binders are removed by incubating yeast with anti-AlexaFluor647 magnetic beads and
515 flowed over a magnetic Milltenyi column at 4 °C. A positive selection follows, comprised of
516 incubation with anti-Myc-AlexaFluor647 antibody (1:100 volume:volume) and anti-
517 AlexaFluor647 magnetic beads (1:10 volume:volume) and flowed over a Milltenyi column on a
518 magnet at 4 °C, such that yeast with bound peptide are retained on the column. These yeast
519 are eluted, grown to confluence in at 30 °C in SDCAA media (pH 5), and sub-cultured in at 20 °C
520 SGCAA media (pH 5) at OD600=1 for two days. The first round of selections of doped libraries
521 were conducted on 180 million yeast (SARS-CoV-2 library) or 400 million yeast (dengue library)
522 to ensure at least 20-fold coverage or peptides. Subsequent rounds of doped library selection,
523 and all rounds of undoped library selections, were performed on 20-25 million yeast.
524
525 *Library sequencing and analysis*
526 Libraries were deep sequenced to determine their composition after each round of
527 selection. Plasmid DNA was extracted from ten million yeast from each round of selection using
528 the Zymoprep Yeast Miniprep Kit (Zymo Research), following manufacturer instructions.
529 Amplicons were generated through PCR, covering the peptide sequence through the 3C cut site.
530 A second PCR round was performed to add i5 and i7 sequencing handles and in-line index
531 barcodes unique to each round of selection. Amplicons were sequenced on an Illumina MiSeq
532 using paired-end MiSeq v2 300bp kits at the MIT BioMicroCenter.
533 Paired-end reads were assembled using PandaSeq (Masella et al., 2012). Peptide
534 sequences were extracted by identifying correctly encoded flanking regions, and were filtered
535 to ensure they matched designed members of the library or the randomized null construct
536 encoding, providing a stringent threshold for contamination and PCR and read errors.
537
538 *Register inference and sequence logos*
539 The 9mer core of enriched sequences was inferred using an in-house alignment
540 algorithm. In this approach, we utilize a 9mer position weight matrix (PWM), which we assess
541 at different offsets along the peptide. We one-hot encode sequences and pad with zeros on the
542 C-terminus of the peptide; to assess seven native registers and four non-native registers, we
543 pad the peptides with four zeros. Three of the non-native registers utilize the linker at the P9
544 anchor but not the P6 anchor, and the addition of a fourth register captures a minority set of
545 peptides which utilize Gly-Gly-Ser-Gly of the linker at P6 through P9 in the groove. Register-
546 setting is performed with zero-padded 15mers, rather than 15mers flanked by invariant
547 flanking residues, because the PWM would otherwise align all sequences to the invariant
548 region.

549 At the start, we randomly assign peptides to registers and generate a 9mer PWM. Over
550 subsequent iterations, peptides are assigned to new registers and the PWM was updated.
551 Assignments are random but biased, such that clusters corresponding to registers that match
552 the PWM are favored. Specifically, at each assignment we first take out the sequence under
553 consideration from the PWM. The PWM then defines an energy value for each register shift of a
554 given peptide, which is then used to generate a Boltzmann distribution from which we sample
555 the updated register shift. The stochasticity is decreased over time by raising the inverse
556 temperature linearly from 0.05 to 1 over 60 iterations, simulating 'cooling' (Andreatta et al.,
557 2017). A final deterministic iteration was carried out, where the distribution concentrates
558 entirely on the optimal register shift.
559 After register inference, sequence logo visualizations of the 9mer cores were generated
560 using Seq2Logo-2.0 with default settings, except using background frequencies from the SARS-
561 CoV-2 proteome and SARS-CoV spike and nucleocapsid proteins (Thomsen and Nielsen, 2012).
562 For registers with the C-terminus utilizing the C-terminal linker, the relevant linker sequence
563 was added to achieve a full 9mer sequence for visualizing the full 9mer core. For HLA-DR401,
564 distribution among registers, starting from N-terminally to C-terminally aligned in the peptide,
565 is: 161, 237, 227, 238, 231, 279, 237, 266, 271, 202, 118.
566
567 *Recombinant protein expression*
568 HLA-DM and HLA-DR401 were expressed recombinantly in High Five insect cells (Thermo
569 Fisher) using a baculovirus expression system, as previously described (Birnbaum et al., 2014;
570 Rappazzo et al., 2020). Ectodomain sequences of each chain were formatted with a C-terminal
571 poly-histidine purification tag and cloned into pAcGP67a vectors. Each vector was individually
572 transfected into SF9 insect cells (Thermo Fisher) with BestBac 2.0 linearized baculovirus DNA
573 (Expression Systems; Davis, CA) and Cellfectin II Reagent (Thermo Fisher), and propagated to
574 high titer. Viruses were co-titrated for optimal expression to maximize balanced MHC
575 heterodimer formation, co-transduced into Hi5 cells, and grown for 48-72 hours at 27 °C. The
576 secreted protein was purified from pre-conditioned media supernatant with Ni-NTA resin and
577 purified via size exclusion chromatography with a S200 increase column on an AKTA PURE FPLC
578 (GE Healthcare). To improve protein yields, the HLA-DRB1*04:01 chain was expressed with a
579 $CLIP_{87\text{-}101}$ peptide (PVSKMRMATPLLMQA) connected to the N-terminus of the MHC chain via a
580 flexible, 3C protease-cleavable linker.
581
582 *Fluorescence polarization experiments for peptide IC_{50} determination*
583 Peptide IC_{50} values were determined following a protocol modified from Yin & Stern (Yin
584 and Stern, 2014), as in Rappazzo et al (Rappazzo et al., 2020). In the assay, recombinantly
585 expressed HLA-DR401 is incubated with fluorescently labelled modified $HA_{306\text{-}318}$ (APRFV{Lys(5,6
586 FAM)}QNTLRLATG) peptide and a titration series for each unlabeled competitor peptide is
587 added (1.28 nM – 20 uM). A change in polarization value resulting from displacement of
588 fluorescent peptide from the binding groove is used to determine IC_{50} values.
589 Relative binding at each concentration is calculated as $(FP_{sample} – FP_{free})/(FP_{no_comp} –$
590 $FP_{free})$. Here, FP_{free} is the polarization value for the fluorescent peptide alone with no added
591 MHC, FP_{no_comp} is polarization value for MHC with no competitor peptide added, and FP_{sample} is
592 the polarization value with both MHC and competitor peptide added. Relative binding curves

were then generated and fit in Prism 9.3 to the equation $y = 1/(1+[pep]/IC_{50})$, where [pep] is the concentration of un-labelled competitor peptide, in order to determine the concentration of half-maximal inhibition, the IC_{50} value.

Each assay was performed at 200 uL, with 100 nM recombinant MHC, 25 nM fluorescent peptide, and competitor peptide (GenScript). This mixture co-incubates in pH 5 binding buffer at 37 °C for 72 hours in black flat bottom 96-well plates. Competitor peptide concentrations ranged from 1.28 nM to 20 µM, as a five-fold dilution series. Three replicates are performed for each peptide concentration. Fluorescent peptide-only, no competitor peptide, and binding buffer controls were also included. Our MHC was expressed with a linked CLIP peptide, so prior to co-incubation, the peptide linker is cleaved by addition of 3C protease at 1:10 molar ratio at room temperature for one hour; the residual cleaved 100 nM CLIP peptide is not expected to alter peptide binding measurements.

Measurements were taken on a Molecular Devices SpectraMax M5 instrument. G-value was 1.1 for each plate, as calculated per manufacturer instructions for each plate based on fluorescent peptide-only wells minus buffer blank wells, with 35 mP reference for 5,6FAM (Fluorescein setting). Measurements were made with 470 nm excitation and 520 nm emission, 10 flashes per read, and default PMT gain high.

Data Availability

All deep sequencing data are deposited on the Sequence Read Archive (SRA), with accession codes PRJNA806475 [https://www.ncbi.nlm.nih.gov/bioproject/PRJNA806475] and PRJNA708266 [https://www.ncbi.nlm.nih.gov/bioproject/PRJNA708266]

Code Availability

Scripts used for data processing and visualization are publicly available at https://github.com/birnbaumlab/Huisman-et-al-2022.

Acknowledgements

We would like to thank Patrick Holec for feedback on this manuscript, and the MIT BioMicro Center for library sequencing. This work was supported in part by the Koch Institute Support (core) Grant P30-CA14051 from the National Cancer Institute. This work was supported by National Institute of Health (U19-AI110495), the Packard Foundation to M.E.B., a Schmidt Futures grant to D.K.G. and M.E.B., and a National Science Foundation Graduate Research Fellowship to B.D.H.

627 **Figures**

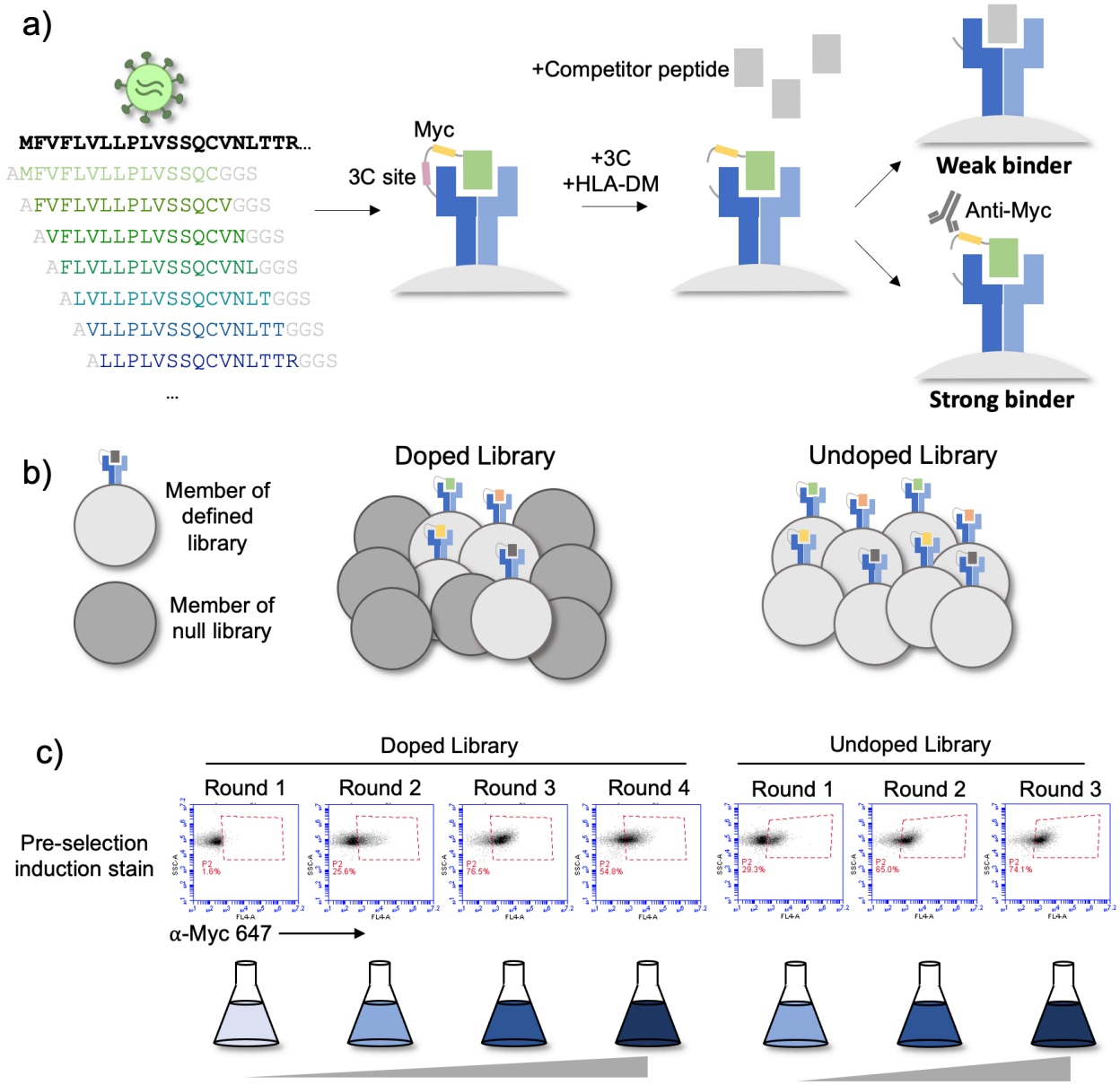

628

629 **Figure 1. Overview of library and selections. a)** The defined library contains pathogen
630 proteome peptides (length 15, sliding window 1). Poor binding peptides are displaced with
631 addition of protease, competitor peptide, and HLA-DM. **b)** Schematic of doped and undoped
632 libraries: in the doped selection strategy, the library is added to a library of null, non-expressing
633 constructs. **c)** Representative flow plots showing enrichment of MHC-expressing yeast over
634 rounds of selection for the library containing SARS-CoV-2 and SARS-CoV peptides on HLA-
635 DR401.

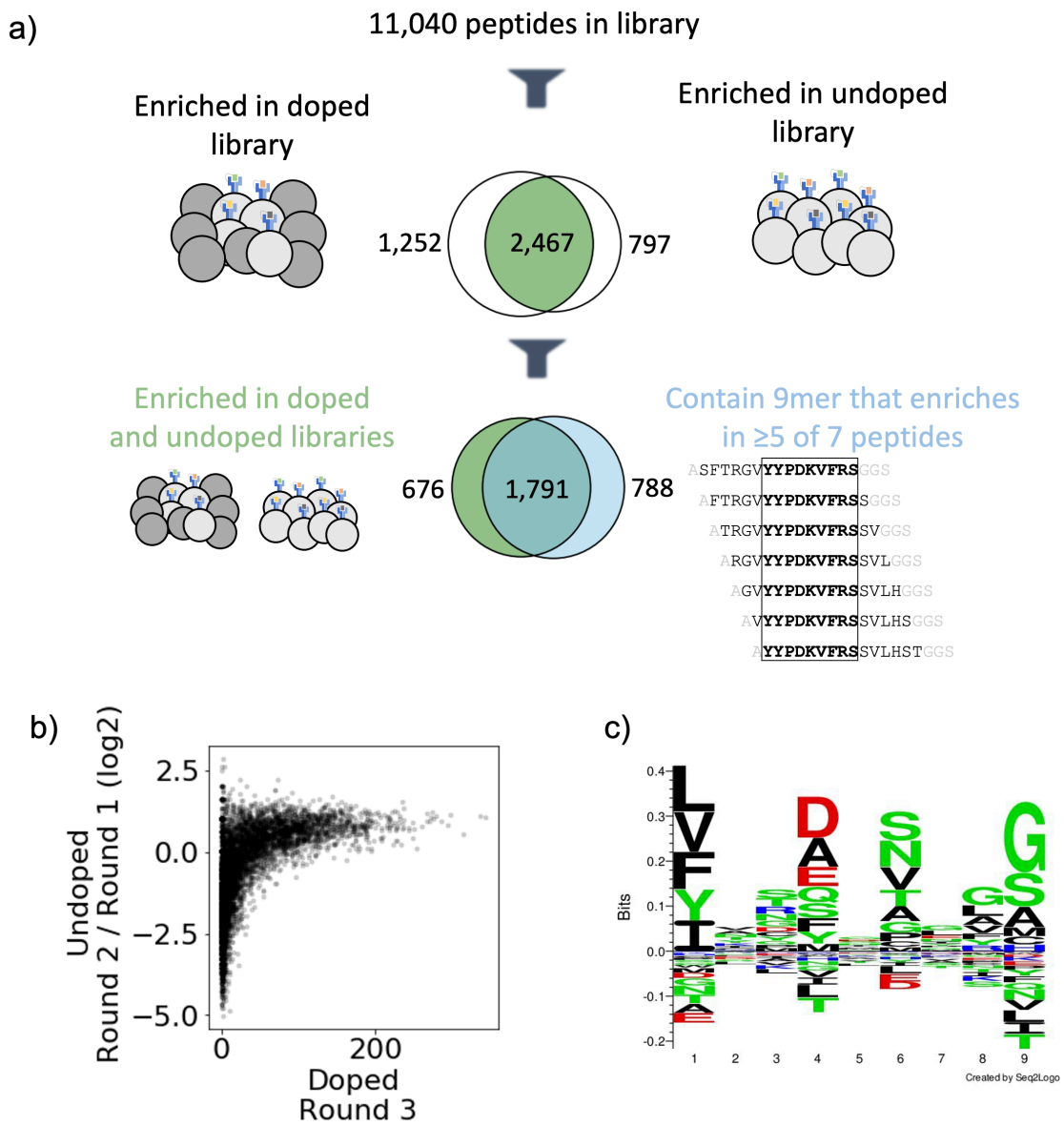

Figure 2. Output of selections and analysis of selection data. a) Overview of filtering peptides and correspondence between selection strategies for SARS-CoV and SARS-CoV-2 library on HLA-DR401. Peptides are filtered for enrichment in both doped and undoped libraries. Further, the relationship between these peptides and peptides which contain a 9mer that is enriched in five or more of the seven peptides containing it is shown. **b)** Relationships between enrichment in doped and undoped libraries. Absolute counts following Round 3 of selection of the doped library are plotted against the log2 fold change between read fraction for peptides in Round 2 and Round 1. Data are shown for the library on HLA-DR401. **c)** Sequence logo of 2,467 peptides that enriched in both doped and undoped selected libraries for HLA-DR401. Registers are inferred with a position weight matrix-based alignment method. Logos were generated with Seq2Logo-2.0.

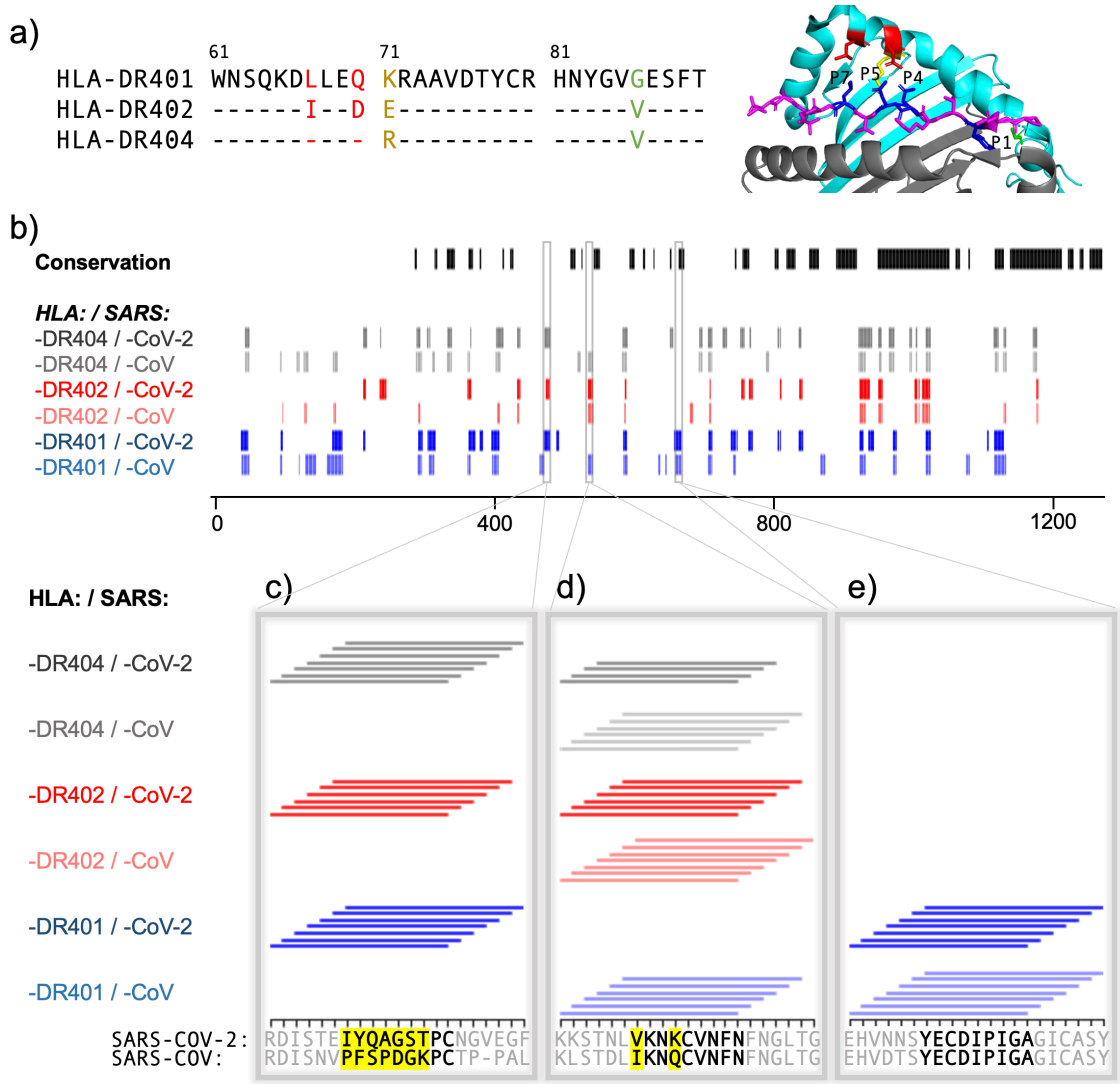

Figure 3. Comparing HLA-DR401, HLA-DR402, and HLA-DR404 for binding to related Spike proteins from SARS-CoV-2 and SARS-CoV. a) Sequence alignment showing sequence differences in HLA-DR402 and HLA-DR404 compared to HLA-DR401 and highlighted on HLA-DR401 structure (PDB 1J8H). Colors are: red for amino acids shared between HLA-DR401 and HLA-DR404, green for amino acids shared between HLA-DR402 and HLA-DR404, and yellow for amino acids different in all 3 alleles. Affected peptide positions (P1, P4, P5, P7) are colored in blue and labeled on the structure. **b)** Conservation and enrichment of 9mer peptides from SARS-CoV-2 and SARS-CoV Spike proteins. Conserved 9mers are indicated in black. If a 9mer along the proteome enriched in 5 or more of the adjacent peptides containing it, its enrichment is indicated with a vertical line with color for allele (HLA-DR401: blue; HLA-DR402: red; HLA-DR404: grey) and opacity for virus (SARS-CoV-2: dark; SARS-CoV: light). **b-e)** Zoomed regions show enrichment of individual 15mer peptides. Only peptides containing the bolded 9mer sequence are shown. Amino acids in the bolded 9mer that are not conserved between SARS-CoV-2 and SARS-CoV are highlighted in yellow.

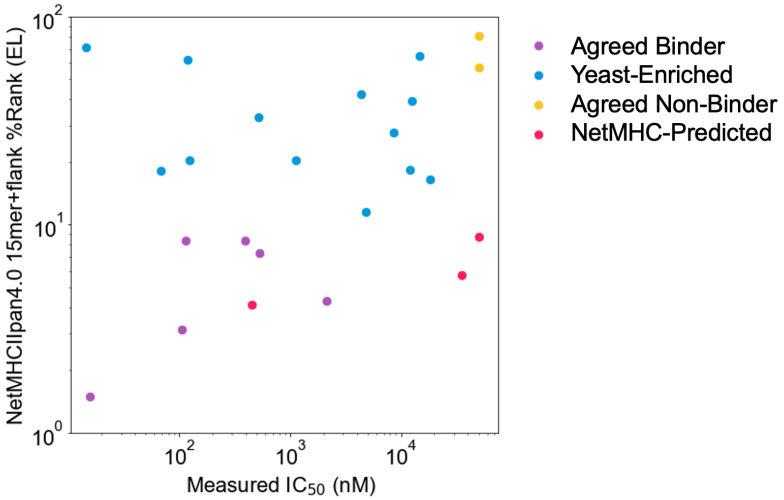

663
664 **Figure 4. Comparing measured IC_{50} values and computational prediction.** Relationship
665 between measured IC_{50} values and NetMHCIIpan4.0 predicted ranks in Eluted Ligand mode (EL)
666 on invariant-flanked sequences. Data points are colored by label, and IC_{50} values ≥50 µM are set
667 to 50 µM.

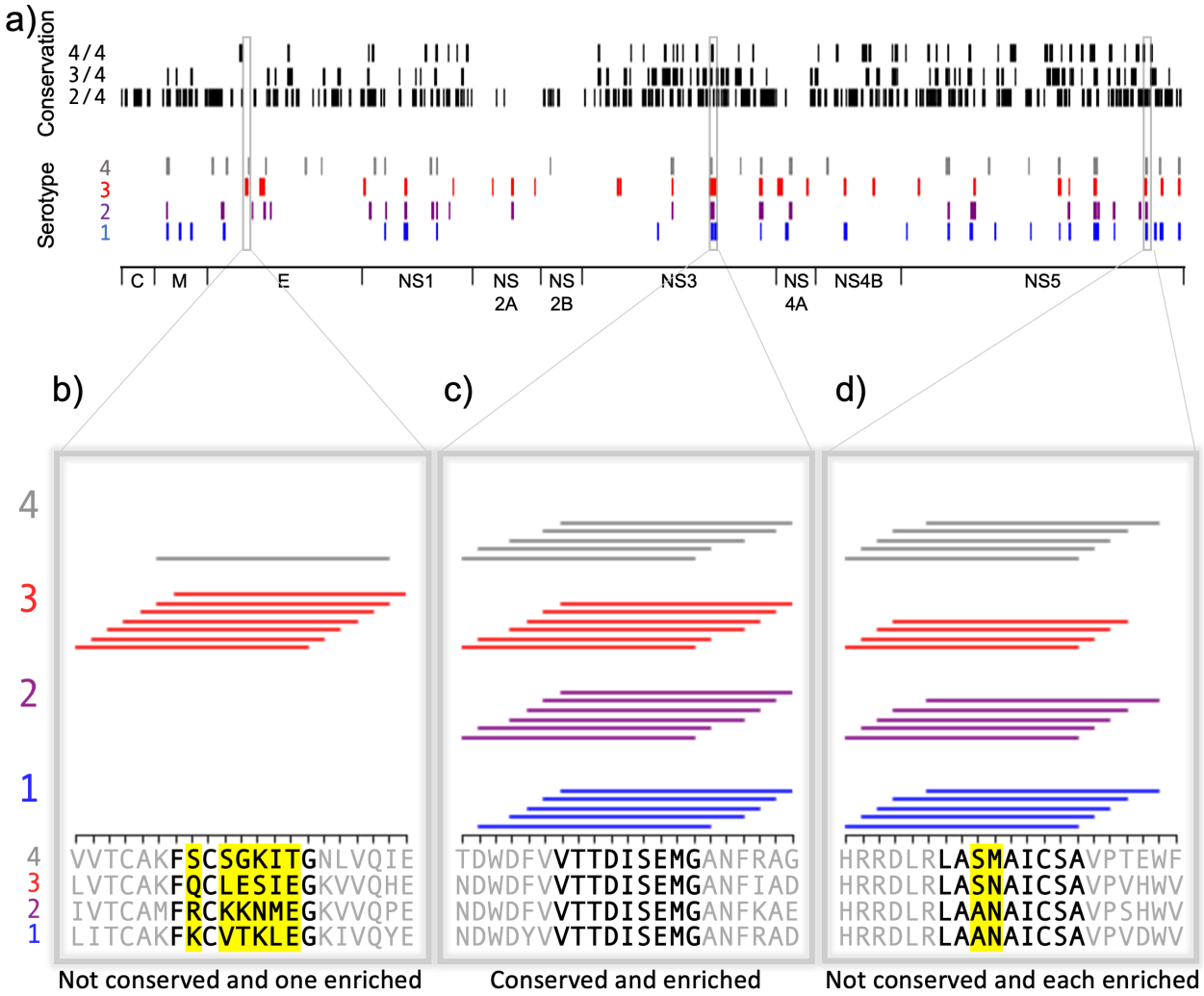

Figure 5. Conservation and enrichment of dengue virus serotypes 1-4. a) Conservation and enrichment of 9mer peptides along four aligned dengue serotypes. All stretches of 9 amino acids are compared across the four serotypes and conservation is indicated with a black vertical line (i.e. 2, 3, or 4 of 4 serotypes conserved). 9mers which enriched on HLA-DR401 are also indicated, colored by virus serotype. **b-d)** Zoomed regions, showing enrichment for individual 15mer peptides to HLA-DR401. Only peptides which contain the bolded 9mer sequence are shown. Amino acids in the bolded 9mer that are not conserved between serotypes are highlighted in yellow. Insets show regions which are differently conserved and enriched: **b)** non-conserved sequences with peptides from one serotype enriched; **c)** conserved sequences enriched across all serotypes; **d)** non-conserved sequences which are enriched.

Virus	Protein	Protein length (# of amino acids)	MHC Allele	# of 15mers	# of 9mer cores	# of smoothed 15mers
SARS-CoV	Spike	1255	HLA-DR401	324	74	221
			HLA-DR402	217	65	110
			HLA-DR404	289	61	193
SARS-CoV	Nucleocapsid	422	HLA-DR401	40	8	34
			HLA-DR402	34	13	12
			HLA-DR404	31	6	20
SARS-CoV-2	Spike	1273	HLA-DR401	305	67	221
			HLA-DR402	230	62	130
			HLA-DR404	290	64	217
SARS-CoV-2	Nucleocapsid	419	HLA-DR401	34	8	24
			HLA-DR402	33	10	15
			HLA-DR404	30	8	18
SARS-CoV-2	Replicase polyprotein 1ab	7096	HLA-DR401	1652	388	1204
			HLA-DR402	1104	325	678
			HLA-DR404	1368	350	890
SARS-CoV-2	Non-structural protein 8	121	HLA-DR401	41	10	32
			HLA-DR402	21	7	17
			HLA-DR404	32	8	19
SARS-CoV-2	Protein 7a	121	HLA-DR401	27	8	18
			HLA-DR402	7	3	0
			HLA-DR404	13	2	6
SARS-CoV-2	Non-structural protein 6	61	HLA-DR401	0	0	0
			HLA-DR402	1	1	0
			HLA-DR404	0	0	0
SARS-CoV-2	Membrane protein	222	HLA-DR401	40	7	29
			HLA-DR402	26	6	19
			HLA-DR404	23	7	21
SARS-CoV-2	Envelope small membrane protein	75	HLA-DR401	6	1	0
			HLA-DR402	7	3	0
			HLA-DR404	6	1	0
SARS-CoV-2	Protein 3a	275	HLA-DR401	22	4	11
			HLA-DR402	13	4	10
			HLA-DR404	10	2	0
SARS-CoV-2	Replicase polyprotein 1a	4405	HLA-DR401	948	228	658
			HLA-DR402	657	196	409
			HLA-DR404	865	222	582
SARS-CoV-2	ORF10 protein	38	HLA-DR401	6	1	6
			HLA-DR402	2	0	0
			HLA-DR404	5	1	5
SARS-CoV-2	Protein non-structural 7b	43	HLA-DR401	0	0	0
			HLA-DR402	0	0	0
			HLA-DR404	0	0	0
SARS-CoV-2	Uncharacterized protein 14	73	HLA-DR401	8	4	6
			HLA-DR402	20	5	16
			HLA-DR404	22	4	21
SARS-CoV-2	Protein 9b	97	HLA-DR401	29	7	27
			HLA-DR402	35	6	31
			HLA-DR404	37	9	34

Table 1. Summary of enriched peptides for each source protein, including: the number of unique 15mers which each enriched in both of the doped and undoped libraries; the number of unique 9mers cores identified by register-inference in these enriched 15mers (native cores only, so linker-containing inferred cores excluded); and the number of unique enriched 15mers that contain 9mer sequences enriched in five or more of overlapping neighbors.

	Spike Position	Peptide+flank (A+15mer+GGS)	NetMHCIIpan4.0 Predicted Core (A+15mer+GGS)	NetMHCIIpan4.0 %Rank (A+15mer+GGS)	15mer Affinity from FP (IC_{50}, nM)
Agreed Binders	34-48	ARGVYYPDKVFRSSVLGGS	YYPDKVFRS	1.49	15.8
	87-101	ANDGVYFASTEKSNIIGGS	VYFASTEKS	4.28	2117
	303-317	ALKSFTVEKGIYQTSNGGS	FTVEKGIYQ	8.41	396.9
	362-376	AVADYSVLYNSASFSTGGS	YSVLYNSAS	8.36	113.7
	1015-1029	AAAEIRASANLAATKMGGS	IRASANLAA	3.13	105.4
	1112-1126	APQIITTDNTFVSGNCGGS	ITTDNTFVS	7.32	527.0
Yeast-Enriched Binders	165-179	ANCTFEYVSQPFLMDLGGS	YVSQPFLMD	64.83	14,652
	172-186	ASQPFLMDLEGKQGNFGGS	FLMDLEGKQ	20.34	123.2
	286-300	ATDAVDCALDPLSETKGGS	VDCALDPLS	32.68	521.6
	373-387	ASFSTFKCYGVSPTKLGGS	YGVSPTKLG	16.59	18,452
	469-483	ASTEIYQAGSTPCNGVGGS	IYQAGSTPC	18.22	67.7
	580-594	AQTLEILDITPCSFGGGGS	LEILDITPC	62	119.9
	739-753	ATMYICGDSTECSNLLGGS	YICGDSTEC	70.91	14.4
	920-934	AQKLIANQFNSAIGKIGGS	FNSAIGKIG	20.47	1121
NetMHC-Predicted Binders	1151-1165	AELDKYFKNHTSPDVDGGS	YFKNHTSPD	5.74	35,510
	492-506	ALQSYGFQPTNGVGYQGGS	YGFQPTNGV	4.11	454.7
	113-127	AKTQSLLIVNNATNVVGGS	IVNNATNVV	8.74	>50,000
Agreed Non-Binders	534-548	AVKNKCVNFNFNGLTGGGS	FNFNGLTGG	57.13	>50,000
	1079-1093	APAICHDGKAHFPREGGGS	ICHDGKAHF	80.47	>50,000

Table 2. Peptides selected for fluorescence polarization (FP) experiments for binding to HLA-DR401. NetMHCIIpan4.0 predictions for HLA-DR401 binding are performed on 15mers plus invariant flanking residues (N-terminal Ala, C-terminal Gly-Gly-Ser) and percent rank values generated using Eluted Ligand mode. Fluorescence polarization is performed on native 15mer peptides without invariant flanking residues.

691

Spike Position	Sequence	NetMHCIIpan4.0 Predicted Core (A+15mer+GGS)	NetMHCIIpan4.0 %Rank (A+15mer+GGS)	NetMHCIIpan4.0 Predicted Core (15mer)	NetMHCIIpan4.0 %Rank (15mer)	15mer Affinity from FP (IC50, nM)
172-186	**SQPFLMDLEGKQGNF**	FLMDLEGKQ	20.34	FLMDLEGKQ	4.1	123.2
173-187	**QPFLMDLEGKQGNFK**	FLMDLEGKQ	27.73	FLMDLEGKQ	12.21	8613
286-300	**TDAVDCALDPLSETK**	VDCALDPLS	32.68	VDCALDPLS	9.8	1154
287-301	**DAVDCALDPLSETKC**	VDCALDPLS	42.42	VDCALDPLS	22.57	4393
469-483	**STEIYQAGSTPCNGV**	IYQAGSTPC	18.22	IYQAGSTPC	5.41	67.7
467-481	**DISTEIYQAGSTPCN**	IYQAGSTPC	11.47	IYQAGSTPC	12.61	4875
471-485	**EIYQAGSTPCNGVEG**	YQAGSTPCN	39.17	YQAGSTPCN	21.81	12519
920-934	**QKLIANQFNSAIGKI**	FNSAIGKIG	20.47	IANQFNSAI	7.89	1495
921-935	**KLIANQFNSAIGKIQ**	FNSAIGKIQ	18.3	IANQFNSAI	19.79	11937

692

693 **Table 3.** Effects of peptide flanking sequences on NetMHCIIpan4.0 predictions for HLA-DR401
694 binding and measured fluorescence polarization (FP) values for overlapping peptides. Yeast
695 display-enriched peptides that are predicted to bind by NetMHCIIpan4.0 when without flanking
696 residues, plus offset variants of these peptides, which are not predicted to bind, with or
697 without flanking sequence. Yeast display register-inferred consensus cores are highlighted in
698 green. NetMHCIIpan4.0 percent rank values are generated using Eluted Ligand mode.

699 **References**

700 Abelin, J.G., Keskin, D.B., Sarkizova, S., Hartigan, C.R., Zhang, W., Sidney, J., Stevens, J., Lane, W.,
701 Zhang, G.L., Eisenhaure, T.M., et al. (2017). Mass spectrometry profiling of HLA-associated
702 peptidomes in mono-allelic cells enables more accurate Epitope prediction. Immunity *46*, 315–
703 326.

704 Abelin, J.G., Harjanto, D., Malloy, M., Suri, P., Colson, T., Goulding, S.P., Creech, A.L., Serrano,
705 L.R., Nasir, G., Nasrullah, Y., et al. (2019). Defining HLA-II ligand processing and binding rules
706 with mass spectrometry enhances cancer Epitope prediction. Immunity *51*, 766-779.e17.

707 Altmann, D.M., and Boyton, R.J. (2020). SARS-CoV-2 T cell immunity: Specificity, function,
708 durability, and role in protection. Sci. Immunol. *5*, eabd6160.

709 Andreatta, M., Alvarez, B., and Nielsen, M. (2017). GibbsCluster: unsupervised clustering and
710 alignment of peptide sequences. Nucleic Acids Res. *45*, W458–W463.

711 Barra, C., Alvarez, B., Paul, S., Sette, A., Peters, B., Andreatta, M., Buus, S., and Nielsen, M.
712 (2018). Footprints of antigen processing boost MHC class II natural ligand predictions. Genome
713 Med. *10*, 84.

714 Birnbaum, M.E., Mendoza, J.L., Sethi, D.K., Dong, S., Glanville, J., Dobbins, J., Ozkan, E., Davis,
715 M.M., Wucherpfennig, K.W., and Garcia, K.C. (2014). Deconstructing the peptide-MHC
716 specificity of T cell recognition. Cell *157*, 1073–1087.

717 Birnbaum, M.E., Mendoza, J., Bethune, M., Baltimore, D., and Garcia, K.C. (2017). Ligand
718 discovery for t cell receptors. US20170192011A1.

719 Dai, Z., Huisman, B.D., Zeng, H., Carter, B., Jain, S., Birnbaum, M.E., and Gifford, D.K. (2021).
720 Machine learning optimization of peptides for presentation by class II MHCs. Bioinformatics.

721 Gambino, F., Jr, Tai, W., Voronin, D., Zhang, Y., Zhang, X., Shi, J., Wang, X., Wang, N., Du, L., and
722 Qiao, L. (2021). A vaccine inducing solely cytotoxic T lymphocytes fully prevents Zika virus
723 infection and fetal damage. Cell Rep. *35*, 109107.

724 Gee, M.H., Han, A., Lofgren, S.M., Beausang, J.F., Mendoza, J.L., Birnbaum, M.E., Bethune, M.T.,
725 Fischer, S., Yang, X., Gomez-Eerland, R., et al. (2018). Antigen identification for orphan T cell
726 receptors expressed on tumor-infiltrating lymphocytes. Cell *172*, 549-563.e16.

727 Guzman, M.G., Gubler, D.J., Izquierdo, A., Martinez, E., and Halstead, S.B. (2016). Dengue
728 infection. Nat. Rev. Dis. Primers *2*, 16055.

729 Hennecke, J., and Wiley, D.C. (2002). Structure of a complex of the human alpha/beta T cell
730 receptor (TCR) HA1.7, influenza hemagglutinin peptide, and major histocompatibility complex
731 class II molecule, HLA-DR4 (DRA*0101 and DRB1*0401): insight into TCR cross-restriction and
732 alloreactivity. J. Exp. Med. *195*, 571–581.

733 Jiang, W., and Boder, E.T. (2010). High-throughput engineering and analysis of peptide binding
734 to class II MHC. Proc. Natl. Acad. Sci. U. S. A. *107*, 13258–13263.

735 Jones, E.Y., Fugger, L., Strominger, J.L., and Siebold, C. (2006). MHC class II proteins and disease:
736 a structural perspective. Nat. Rev. Immunol. *6*, 271–282.

737 Justesen, S., Harndahl, M., Lamberth, K., Nielsen, L.-L.B., and Buus, S. (2009). Functional
738 recombinant MHC class II molecules and high-throughput peptide-binding assays. Immunome
739 Res. *5*, 2.

740 Karnes, J.H., Bastarache, L., Shaffer, C.M., Gaudieri, S., Xu, Y., Glazer, A.M., Mosley, J.D., Zhao,
741 S., Raychaudhuri, S., Mallal, S., et al. (2017). Phenome-wide scanning identifies multiple
742 diseases and disease severity phenotypes associated with HLA variants. Sci. Transl. Med. *9*.

743 Keskin, D.B., Anandappa, A.J., Sun, J., Tirosh, I., Mathewson, N.D., Li, S., Oliveira, G., Giobbie-
744 Hurder, A., Felt, K., Gjini, E., et al. (2019). Neoantigen vaccine generates intratumoral T cell
745 responses in phase Ib glioblastoma trial. Nature *565*, 234–239.

746 Klinger, M., Pepin, F., Wilkins, J., Asbury, T., Wittkop, T., Zheng, J., Moorhead, M., and Faham,
747 M. (2015). Multiplex Identification of Antigen-Specific T Cell Receptors Using a Combination of
748 Immune Assays and Immune Receptor Sequencing. PLoS One *10*, e0141561.

749 Liu, G., Carter, B., Bricken, T., Jain, S., Viard, M., Carrington, M., and Gifford, D.K. (2020).
750 Computationally optimized SARS-CoV-2 MHC class I and II vaccine formulations predicted to
751 target human haplotype distributions. Cell Syst. *11*, 131-144.e6.

752 Liu, G., Carter, B., and Gifford, D.K. (2021a). Predicted cellular immunity population coverage
753 gaps for SARS-CoV-2 subunit vaccines and their augmentation by compact peptide sets. Cell
754 Syst. *12*, 102-107.e4.

755 Liu, R., Jiang, W., and Mellins, E.D. (2021b). Yeast display of MHC-II enables rapid identification
756 of peptide ligands from protein antigens (RIPPA). Cell. Mol. Immunol. *18*, 1847–1860.

757 Lovitch, S.B., Pu, Z., and Unanue, E.R. (2006). Amino-terminal flanking residues determine the
758 conformation of a peptide-class II MHC complex. J. Immunol. *176*, 2958–2968.

759 Madeira, F., Park, Y.M., Lee, J., Buso, N., Gur, T., Madhusoodanan, N., Basutkar, P., Tivey,
760 A.R.N., Potter, S.C., Finn, R.D., et al. (2019). The EMBL-EBI search and sequence analysis tools
761 APIs in 2019. Nucleic Acids Res. *47*, W636–W641.

762 Masella, A.P., Bartram, A.K., Truszkowski, J.M., Brown, D.G., and Neufeld, J.D. (2012).
763 PANDAseq: paired-end assembler for illumina sequences. BMC Bioinformatics *13*, 31.

764 Mateus, J., Grifoni, A., Tarke, A., Sidney, J., Ramirez, S.I., Dan, J.M., Burger, Z.C., Rawlings, S.A.,
765 Smith, D.M., Phillips, E., et al. (2020). Selective and cross-reactive SARS-CoV-2 T cell epitopes in
766 unexposed humans. Science *370*, 89–94.

767 Moise, L., Gutierrez, A., Kibria, F., Martin, R., Tassone, R., Liu, R., Terry, F., Martin, B., and De
768 Groot, A.S. (2015). iVAX: An integrated toolkit for the selection and optimization of antigens
769 and the design of epitope-driven vaccines. Hum. Vaccin. Immunother. *11*, 2312–2321.

770 Obermair, F.J., Renoux, F., Heer, S., Lee, C., Cereghetti, N., Maestri, G., Haldner, Y., Wuigk, R.,
771 Iosefson, O., Patel, P., et al. (2021). High resolution profiling of MHC-II peptide presentation
772 capacity, by Mammalian Epitope Display, reveals SARS-CoV-2 targets for CD4 T cells and
773 mechanisms of immune-escape (bioRxiv).

774 O'Brien, C., Flower, D.R., and Feighery, C. (2008). Peptide length significantly influences in vitro
775 affinity for MHC class II molecules. Immunome Res. *4*, 6.

776 O'Donnell, T.J., Rubinsteyn, A., and Laserson, U. (2020). MHCflurry 2.0: Improved pan-allele
777 prediction of MHC class I-presented peptides by incorporating antigen processing. Cell Syst. *11*,
778 42-48.e7.

779 Ott, P.A., Hu, Z., Keskin, D.B., Shukla, S.A., Sun, J., Bozym, D.J., Zhang, W., Luoma, A., Giobbie-
780 Hurder, A., Peter, L., et al. (2017). An immunogenic personal neoantigen vaccine for patients
781 with melanoma. Nature *547*, 217–221.

782 Parker, R., Partridge, T., Wormald, C., Kawahara, R., Stalls, V., Aggelakopoulou, M., Parker, J.,
783 Powell Doherty, R., Ariosa Morejon, Y., Lee, E., et al. (2021). Mapping the SARS-CoV-2 spike
784 glycoprotein-derived peptidome presented by HLA class II on dendritic cells. Cell Rep. *35*,
785 109179.

786 Patronov, A., and Doytchinova, I. (2013). T-cell epitope vaccine design by immunoinformatics.
787 Open Biol. *3*, 120139.

788 Purcell, A.W., Ramarathinam, S.H., and Ternette, N. (2019). Mass spectrometry-based
789 identification of MHC-bound peptides for immunopeptidomics. Nat. Protoc. *14*, 1687–1707.

790 Racle, J., Michaux, J., Rockinger, G.A., Arnaud, M., Bobisse, S., Chong, C., Guillaume, P., Coukos,
791 G., Harari, A., Jandus, C., et al. (2019). Robust prediction of HLA class II epitopes by deep motif
792 deconvolution of immunopeptidomes. Nat. Biotechnol. *37*, 1283–1286.

793 Rappazzo, C.G., Huisman, B.D., and Birnbaum, M.E. (2020). Repertoire-scale determination of
794 class II MHC peptide binding via yeast display improves antigen prediction. Nat. Commun. *11*,
795 4414.

796 Reynisson, B., Alvarez, B., Paul, S., Peters, B., and Nielsen, M. (2020). NetMHCpan-4.1 and
797 NetMHCIIpan-4.0: improved predictions of MHC antigen presentation by concurrent motif
798 deconvolution and integration of MS MHC eluted ligand data. Nucleic Acids Res. *48*, W449–
799 W454.

800 Rosati, E., Pogorelyy, M.V., Minervina, A.A., Scheffold, A., Franke, A., Bacher, P., and Thomas,
801 P.G. (2021). Characterization of SARS-CoV-2 public CD4+ αβ T cell clonotypes through reverse
802 epitope discovery. BioRxivorg.

803 Sidney, J., Steen, A., Moore, C., Ngo, S., Chung, J., Peters, B., and Sette, A. (2010). Divergent
804 motifs but overlapping binding repertoires of six HLA-DQ molecules frequently expressed in the
805 worldwide human population. J. Immunol. *185*, 4189–4198.

806 Snyder, T.M., Gittelman, R.M., Klinger, M., May, D.H., Osborne, E.J., Taniguchi, R., Zahid, H.J.,
807 Kaplan, I.M., Dines, J.N., Noakes, M.T., et al. (2020). Magnitude and dynamics of the T-cell
808 response to SARS-CoV-2 infection at both individual and population levels. MedRxiv.

809 Stern, L.J. (1994). Crystal structure of the human class II MHC protein HLA- DR1 complexed with
810 an influenza virus peptide. Nature *368*, 215–221.

811 Stopfer, L.E., Mesfin, J.M., Joughin, B.A., Lauffenburger, D.A., and White, F.M. (2020).
812 Multiplexed relative and absolute quantitative immunopeptidomics reveals MHC I repertoire
813 alterations induced by CDK4/6 inhibition. Nat. Commun. *11*, 2760.

814 Stopfer, L.E., Gajadhar, A.S., Patel, B., Gallien, S., Frederick, D.T., Boland, G.M., Sullivan, R.J., and
815 White, F.M. (2021). Absolute quantification of tumor antigens using embedded MHC-I
816 isotopologue calibrants. Proc. Natl. Acad. Sci. U. S. A. *118*, e2111173118.

817 Thomsen, M.C.F., and Nielsen, M. (2012). Seq2Logo: a method for construction and
818 visualization of amino acid binding motifs and sequence profiles including sequence weighting,
819 pseudo counts and two-sided representation of amino acid enrichment and depletion. Nucleic
820 Acids Res. *40*, W281-7.

821 Vita, R., Mahajan, S., Overton, J.A., Dhanda, S.K., Martini, S., Cantrell, J.R., Wheeler, D.K., Sette,
822 A., and Peters, B. (2019). The Immune Epitope Database (IEDB): 2018 update. Nucleic Acids Res.
823 *47*, D339–D343.

824 Yin, L., and Stern, L.J. (2014). Measurement of peptide binding to MHC class II molecules by
825 fluorescence polarization. Curr. Protoc. Immunol. *106*, 5.10.1-5.10.12.

826 Zavala-Ruiz, Z., Strug, I., Anderson, M.W., Gorski, J., and Stern, L.J. (2004). A polymorphic pocket
827 at the P10 position contributes to peptide binding specificity in class II MHC proteins. Chem.
828 Biol. *11*, 1395–1402.

829 Zeng, H., and Gifford, D.K. (2019). Quantification of uncertainty in peptide-MHC binding
830 prediction improves high-affinity peptide selection for therapeutic design. Cell Syst. *9*, 159-
831 166.e3.

832 Zhao, W., and Sher, X. (2018). Systematically benchmarking peptide-MHC binding predictors:
833 From synthetic to naturally processed epitopes. PLoS Comput. Biol. *14*, e1006457.